Distorted-Wave Calculation of Electron-Impact Excitation of Atomic Oxygen*

T. Sawada and P. S. Ganas†
University of Florida, Gainesville, Florida 32601
(Received 22 September 1972; revised manuscript received 8 November 1972)

A distorted-wave formulation with exchange is given for the electron-impact excitation of atoms from $(n_0l_0)^N$ to $(n_0l_0)^{N-1}nl$ configurations using the LS-coupling scheme. Phenomenologically determined independent-particle models and distorted-wave potentials are utilized to compute angular distributions and integrated cross sections for $2p \rightarrow 3s$, $3p$, and $4p$ excitations of atomic oxygen over wide ranges of energy and momentum transfer. The results are compared with the Born-approximation limit as well as the experimental integrated cross section of Stone and Zipf.

I. INTRODUCTION

Atomic oxygen plays a major role in the understanding of auroral, dayglow, and ionospheric phenomena which require a detailed knowledge of electron-impact cross sections, among other things, for their explanation. There have been a number of theoretical studies of electron-impact excitation of atomic oxygen, and excellent reviews of the subject can be found, for example, in the review article by Moiseiwitsch and Smith[1] and in the monograph by Massey and Burhop.[2] The excitation of the ^1D and ^1S states of the ground-state configuration $1s^22s^22p^4$ from the ground ^3P state by slow electrons has received considerable attention. Yamanouchi *et al.*,[3] Seaton,[4] Smith *et al.*,[5] and Henry *et al.*[6] have calculated integrated cross sections using Hartree–Fock wave functions both in the distorted-wave (DW) approximation[3,4] and in the close-coupling approach.[4–6] It has been established by Bates *et al.*[7] and by Seaton[4] that the basic assumption of weak coupling inherent in the DW calculation was invalid in the excitation of the ^1D and ^1S states because they lie too close to the ground ^3P state.

In this work, we apply the DW approximation to the electron-impact excitation of atomic oxygen from the ground state to the $3s(^3S, ^5S)$, $3p(^3P, ^5P)$, and $4p(^3P, ^5P)$ states, assuming that the core is frozen to the ^4S state of the $1s^22s^22p^3$ configuration. We expect that the coupling between the ground state and these excited states is sufficiently weak that the DW calculation is valid. We base this assumption on the fact that the energy separations between the ground and excited states are large, and that these transitions involve the change of one electron orbital, in contrast to the transitions among the ^3P, ^1D, and ^1S lowest levels.

The DW and exchange-DW Born–Oppenheimer approximations have been applied by Percival[8] to compute the collision strengths of the excitation of $3p(^3P$ and $^5P)$ states at very low incident energies using Hartree–Fock wave functions. The integrated cross section for the $2p(^3P) \rightarrow 3s(^3S)$ transition over a wide range of energy has been calculated by Stauffer and McDowell[9] with an impact-parameter method using Hartree–Fock wave functions.

Here we base our computation on the independent-particle model (IPM) of Green and his collaborators.[10–15] In comparison to Hartree–Fock–Slater calculations and to experiment, a simple two-parameter model has been found to provide a good representation of atoms and electron-atom interactions. The present DW calculation is an extension of the previous work on Ne and Ar by Sawada, Purcell, and Green (SPG).[13] As in SPG, we assume the LS-coupling scheme for both the ground state and excited states. For moderately highly excited states, it may be more accurate to utilize the Jl-coupling scheme. A detailed formulation has been given by Shelton and Leherissey[16] for the transitions from the LS-coupled ground state to a Jl-coupled excited state for the rare gases. Here, however, as in SPG, we simply assume that the LS coupling is valid, and ignore any spin-orbit couplings that cause fine-structure splittings.

In the examples cited above[3–9] on atomic oxygen, no attention has been given to angular distributions of the projectile electron. For a microscopic study of electron energy deposition, for example, the spatial distribution of scattered electrons as well as their energy distribution is expected to play important roles. Owing to the difficulty in studying these collisions experimentally, there have been no data available on angular distributions so far, and some sort of reasonably reliable theoretical predictions seem worth presenting.

The electron-impact excitation and ionization of atomic oxygen has recently been studied in the Born approximation by Kazaks, Ganas, and Green[15] (KGG) using an analytic atomic IPM potential which reproduces the 15 excited single-particle levels from $3s$ to $8s$, $3p$ to $6p$, and $3d$ to $7d$ in close agreement with the experimental energies. Their results for integrated cross sections were generally

in good agreement with experiment above 100 eV. In order to extend their work to lower-energy regions, and to obtain more realistic angular distributions, it is necessary to include the effects of distortion as well as exchange. The present DW calculation utilizes the KGG potential to construct the atomic wave functions.

In Sec. II we present a DW formulation which is a generalization of that given by SPG, and describes excitation from an incomplete subshell. In Sec. III we discuss the choice of the phenomenological distorting potentials in relation to the KGG potential and to the experimental total cross sections of Sunshine *et al.*[17] In Sec. IV, we apply our formulation to calculate angular distributions and integrated cross sections for the various transitions in atomic oxygen which were mentioned earlier. We compare our integrated cross sections with the recent measurements by Stone and Zipf.[18]

II. DISTORTED-WAVE FORMULATION

We suppose that the initial state of the atom is specified by the quantum numbers L_0, S_0, J_0, and M_0. After an electron has been promoted from an n_0l_0 orbital to an nl orbital, the atom is in a final state specified by L, S, J, and M. We suppose that there are N electrons in the n_0l_0 subshell, and that the inert core $(n_0l_0)^{N-1}$ is specified by the quantum numbers L_c, S_c, J_c, and M_c. The projectile electron has initial momentum $\vec{k}_i$ and final momentum $\vec{k}_f$. The differential cross section for the transition $(n_0l_0)^N \to (n_0l_0)^{N-1}nl$ is

$$\sum_J \frac{d\sigma}{d\Omega} = \frac{k_f}{k_i}\left(\frac{m_e}{2\pi\hbar^2}\right)^2 \frac{1}{2J_0+1}\left(\frac{1}{2}\right) \sum_{\substack{JMM_0 \\ m_{s_i}m_{s_f}}} |M^D - NM^E|^2 , \quad (1)$$

where we have summed over contributions from all final states with J that are possible for a given set of S and L. All these states are degenerate in our model. In Eq. (1), M^D and M^E are the amplitudes for the direct and exchange processes, respectively. In the DW approximation,

$$M^D = N\langle \psi_f(\bar{0})\,\chi_f^{(-)}(0)\,|v_{01}|\,\psi_i(\bar{0})\,\chi_i^{(+)}(0)\rangle , \quad (2)$$

$$M^E = \langle \psi_f(\bar{1})\,\chi_f^{(-)}(1)\,|v_{01}|\,\psi_i(\bar{0})\,\chi_i^{(+)}(0)\rangle . \quad (3)$$

Equations (2) and (3) are analogous to Eqs. (2.8) and (2.14) of SPG. In the direct process, electron 0 comes in and is scattered out inelastically; we denote the ground-state and excited-state atomic wave functions by $\psi_i(\bar{0})$ and $\psi_f(\bar{0})$, respectively, indicating that electron 0 is the projectile. In the exchange process, the incident electron 0 drops into the nl orbit, while electron 1 is knocked out from the n_0l_0 orbit; the ground-state and excited-state atomic wave functions are then $\psi_i(\bar{0})$ and $\psi_f(\bar{1})$, respectively. The quantities χ_i^+ and χ_f^- are the distorted waves for an electron in the incident and outgoing channels, respectively, with appropriate boundary conditions at infinity. The normalization of χ_i^+ and χ_f^- is such that in the absence of distorting potentials they are to be replaced by $\exp(i\vec{k}_i\cdot\vec{r})$ and $\exp(i\vec{k}_f\cdot\vec{r})$, respectively. The remarks made in Secs. II and III of SPG on the choice of the distorting potentials apply here also. In Eqs. (2) and (3), v_{ij} is the Coulomb interaction between electrons i and j.

The basic difference between the present formulation and that of SPG lies in the initial and final atomic states. The LS-coupled antisymmetrized initial atomic state for the $(n_0l_0)^N$ configuration is

$$\psi_i(\bar{0}) = \sum_{M_{S_0}M_{L_0}} (S_0M_{S_0}L_0M_{L_0}|J_0M_0)\,F^{S_0L_0}_{S_cL_c} \sum_{M_{S_c}M_{L_c}} \sum_{m_{s_0}m_{l_0}} \sum_{J_cM_c} (S_cM_{S_c}\tfrac{1}{2}m_{s_0}|S_0M_{S_0})\,(L_cM_{L_c}l_0m_{l_0}|L_0M_{L_0})$$
$$\times (S_cM_{S_c}L_cM_{L_c}|J_cM_c)\,\phi(n_0l_0m_{s_0}m_{l_0};\,1)\,\Phi_c(L_cS_cJ_cM_c;\,2,\,3,\,\ldots,\,N) . \quad (4)$$

The LS-coupled antisymmetrized final atomic state for the $(n_0l_0)^{N-1}nl$ configuration is

$$\psi_f(\bar{0}) = \sum_{M_SM_L} (SM_SLM_L|JM) \sum_{M'_{S_c}M'_{L_c}} \sum_{m_sm_l} \sum_{J'_cM'_c} (S'_cM'_{S_c}\tfrac{1}{2}m_s|SM_s)\,(L'_cM'_{L_c}lm_l|LM_L)\,(S'_cM'_{S_c}L'_cM'_{L_c}|J'_cM'_c)\,\frac{1}{\sqrt{N}}$$
$$\times\left(1-\sum_{t=2}^{N}P_{1t}\right)\phi(nlm_sm_l;\,1)\,\Phi_c(L'_cS'_cJ'_cM'_c;\,2,\,3,\,\ldots,\,N) . \quad (5)$$

For $\psi_f(\bar{1})$ we have Eq. (5) with the particle index 1 replaced by 0. In Eqs. (4) and (5), Φ_c describes the antisymmetric wave function of the core electrons, and ϕ describes the extra core electron which couples to the core to produce the initial or final state of the atom. In Eq. (4), $F^{S_0L_0}_{S_cL_c}$ is the coefficient of fractional parentage for constructing the initial state $(n_0l_0)^NS_0L_0$ from the core state $(n_0l_0)^{N-1}S_cL_c$ and an n_0l_0 electron. In Eq. (5), the antisymmetrization is carried out explicitly by the exchange operators P_{ij}. The bracketed quantities such as $(S_0M_{S_0}L_0M_{L_0}|J_0M_0)$ are Clebsch–Gordan coefficients.[19]

As discussed in SPG, it is advantageous for computational economy and accuracy to rewrite Eq. (1) in the form

$$\sum_J \frac{d\sigma}{d\Omega} = \frac{k_f}{k_i}\left(\frac{m_e}{2\pi\hbar^2}\right)^2 \frac{1}{2J_0+1}\left(\frac{1}{2}\right) \times \sum_{JMM_0,m_{s_i}m_{s_f}} |(M^D - M^B) - NM^E + M^B|^2 , \quad (6)$$

where M^B is the Born amplitude. Equation (6) may be expressed in the form

$$\sum_J \frac{d\sigma}{d\Omega} = \gamma[\delta_{SS_0}(T_1+T_2+T_4+T_5+T_6) + T_3] , \quad (7)$$

where

$$\gamma = 4\pi \frac{k_f}{k_i}\left(\frac{m_e e^2}{2\pi\hbar^2}\right)^2 = \left(\frac{1}{\pi}\right)\frac{k_f}{k_i}\, a_0^2 ; \quad (8)$$

$$T_1 = \gamma' \tfrac{1}{2}\sum |M^D - M^B|^2 , \quad (9)$$

$$T_2 = \gamma' \tfrac{1}{2}\sum (-2N)\,\mathrm{Re}(M^D - M^B)M^{E*} , \quad (10)$$

$$T_3 = \gamma' \tfrac{1}{2}\sum N^2 |M^E|^2 , \quad (11)$$

$$T_4 = \gamma' \tfrac{1}{2}\sum 2\mathrm{Re}(M^D - M^B)M^{B*} , \quad (12)$$

$$T_5 = \gamma' \tfrac{1}{2}\sum (-2N)\,\mathrm{Re}M^E M^{B*} , \quad (13)$$

$$T_6 = \gamma' \tfrac{1}{2}\sum |M^B|^2 ; \quad (14)$$

$$\gamma' = (4\pi e^4 \hat{J}_0)^{-1} . \quad (15)$$

Throughout the rest of this work we use the notation $\hat{J}_0 \equiv 2J_0+1$. We present our results in Secs. II A–II F.

A. Direct Amplitude M^D–M^B

We rewrite M^D of Eq. (2) by using Eqs. (4) and (5) and the partial-wave expansions of the distorted waves given by Eqs. (3.5a) and (3.5b) of SPG. The radial parts of the distorted waves, f_l, appearing in the partial-wave expansions are obtained by solving the radial Schrödinger equation with suitably chosen potentials, as discussed in Sec. III. In the resulting expression for M^D we introduce the multipole expansion of v_{01} given by Eq. (3.4) of SPG. Taking advantage of all orthogonalities, we find

$$M^D = \delta_{S S_0}\delta_{m_{s_i} m_{s_f}} \sum_{l_i \lambda l_f m_{l_f}} Y(l_f m_{l_f})(\hat{k}_f)\, i^{l_i - l_f}(\hat{l}_i)^{1/2} \sum_{\text{all } m} (-)^{\lambda + m_l} \begin{pmatrix} S_0 & L_0 & J_0 \\ M_{S_0} & M_{L_0} & -M_0 \end{pmatrix} \begin{pmatrix} L & L_c & l \\ M_L & -M_{L_c} & -m_l \end{pmatrix}$$
$$\times \begin{pmatrix} S_0 & L & J \\ M_{S_0} & M_L & -M \end{pmatrix} \begin{pmatrix} L_0 & L_c & l_0 \\ M_{L_0} & -M_{L_c} & -m_{l_0} \end{pmatrix} \begin{pmatrix} l_f & \lambda & l_i \\ -m_{l_f} & -\mu & 0 \end{pmatrix} \begin{pmatrix} l & \lambda & l_0 \\ -m_l & \mu & m_{l_0} \end{pmatrix}$$
$$\times (\hat{J}_0 \hat{J} \hat{L}_0 \hat{L})^{1/2} (N)^{1/2} (4\pi)^{3/2} F^{S_0 L_0}_{S_c L_c}\, e^2 (\hat{l}_f \hat{l}_i \hat{l} \hat{l}_0)^{1/2} \begin{pmatrix} l_f & \lambda & l_i \\ 0 & 0 & 0 \end{pmatrix} \begin{pmatrix} l & \lambda & l_0 \\ 0 & 0 & 0 \end{pmatrix} (-)^{l_i + l_f} \xi^{\lambda}_{l_i l_f l l_0} , \quad (16)$$

where

$$\xi^{\lambda}_{l_i l_f l l_0} = \langle f^*_{l_f}(k_f, r_0) R_{nl}(r_1) | r_<^{\lambda}/r_>^{\lambda+1} | R_{n_0 l_0}(r_1) f_{l_i}(k_i, r_0) \rangle . \quad (17)$$

In Eq. (17), $R_{nl}(r_1)$ and $R_{n_0 l_0}(r_1)$ are the radial parts of the single-particle bound-state wave functions $\phi(nlm_s m_l; 1)$ and $\phi(n_0 l_0 m_{s_0} m_{l_0}; 1)$, respectively. The bracketed arrays in Eq. (16) are $3j$ symbols. In $\sum_{\text{all } m}$, we sum over all magnetic substates except M and M_0. Although this sum can be performed explicitly, the form (16) is more tractable for calculating T_1.

For M^B that appears in (9), (10), and (12) in the combination $M^D - M^B$, we introduce a quantity analogous to (17):

$$\xi^{B\lambda}_{l_i l_f l l_0} = \langle j_{l_f}(k_f r_0) R_{nl}(r_1) | r_<^{\lambda}/r_>^{\lambda+1} | R_{n_0 l_0}(r_1) j_{l_i}(k_i r_0) \rangle , \quad (18)$$

where $j_l(kr)$ is a spherical Bessel function. Then $M^D - M^B$ is given by Eq. (16), with ξ^{λ} replaced by $\xi^{\lambda} - \xi^{B\lambda}$.

B. Exchange Amplitude M^E

In the exchange amplitude M^E of Eq. (3), we substitute Eqs. (4) and (5), with the electron 0 replaced by the electron 1. As in SPG, we choose for the distorting potential in M^E the same potential from which the bound-state wave functions are computed. Then the scattering states in M^E become orthogonal to the bound states and we may drop the term $\sum_{t=2}^{N} P_{0t}$ in Eq. (5). By taking advantage of all orthogonalities and using the multipole expansion for v_{01}, the exchange amplitude becomes

$$M^E = \sum_{l_i l_f \lambda} \sum_{\text{all } m} Y(l_f m_{l_f})(\hat{k}_f) \begin{pmatrix} S_0 & L_0 & J_0 \\ M_{S_0} & M_{L_0} & -M_0 \end{pmatrix} \begin{pmatrix} S & L & J \\ M_S & M_L & -M \end{pmatrix} \begin{pmatrix} S_c & \frac{1}{2} & S_0 \\ M_{S_c} & m_{s_f} & -M_{S_0} \end{pmatrix} \begin{pmatrix} S_c & \frac{1}{2} & S \\ M_{S_c} & m_{s_i} & -M_S \end{pmatrix} (-)^{l_i + l_f}$$

$$\times\begin{pmatrix} L_c & l_0 & L_0 \\ M_{L_c} & m_{l_0} & -M_{L_0}\end{pmatrix}\begin{pmatrix} L_c & l & L \\ M_{L_c} & m_l & -M_L\end{pmatrix}\begin{pmatrix} l_0 & \lambda & l_f \\ m_{l_0} & \mu & -m_{l_f}\end{pmatrix}\begin{pmatrix} l & \lambda & l_i \\ m_l & \mu & 0\end{pmatrix}(-)^{m_{l_f}}(\hat{J}_0\hat{S}_0\hat{L}_0\hat{J}\hat{S}\hat{L})^{1/2}\left(\frac{1}{N}\right)^{1/2}$$

$$\times(4\pi)^{3/2}i^{l_i-l_f}(\hat{l}_i)^{1/2}e^2(\hat{l}_f\hat{l}_0\hat{l}\hat{l}_i)^{1/2}\begin{pmatrix} l_f & \lambda & l_0 \\ 0 & 0 & 0\end{pmatrix}\begin{pmatrix} l & \lambda & l_i \\ 0 & 0 & 0\end{pmatrix}F^{S_0L_0}_{S_cL_c}(-)^{\omega}\eta^{\lambda}_{l_il_fll_0}\ , \quad (19)$$

where $\omega=-S_0+L_0-S+L+1-2S_c$, and

$$\eta^{\lambda}_{l_il_fll_0}=\langle f^{*}_{l_f}(k_f,r_1)R_{nl}(r_0)\,|r^{\lambda}_{<}/r^{\lambda+1}_{>}|R_{n_0l_0}(r_1)\times f_{l_i}(k_i,r_0)\rangle\ . \quad (20)$$

The notation $\sum_{\text{all } m}$ in Eq. (19) means that we sum over all m's except M, M_0, m_{s_i}, and m_{s_f}. Although this sum can be performed explicitly, the subsequent algebraic manipulations become more tractable if we leave M^E in the form (19).

C. Born Amplitude M^B

For the Born amplitude M^B that appears in (12)–(14) (but not in the combination M^D-M^B), we utilize

$$M^B=N\langle e^{i\vec{k}_f\cdot\vec{r}_1}\psi_f(\bar{0})|v_{01}|\psi_i(\bar{0})\,e^{i\vec{k}_i\cdot\vec{r}_1}\rangle=(4\pi e^2/K^2)N\langle\psi_f(\bar{0})|e^{i\vec{K}\cdot\vec{r}_1}|\psi_i(\bar{0})\rangle\ , \quad (21)$$

where $\vec{K}=\vec{k}_i-\vec{k}_f$ is the momentum transfer. Using Eqs. (4) and (5) and the Rayleigh expansion for $e^{i\vec{K}\cdot\vec{r}_1}$, we find

$$M^B=\delta(SS_0)\,\delta(m_{s_i}m_{s_f})\sum_{\lambda\mu}(-)^M\begin{pmatrix}\lambda & J & J_0\\ \mu & -M & M_0\end{pmatrix}Y^{*}_{\lambda\mu}(\hat{K})\frac{4\pi e^2}{K^2}(N)^{1/2}F^{S_0L_0}_{S_cL_c}i^{\lambda}(4\pi\hat{l}\hat{\lambda}\hat{l}_0)^{1/2}\begin{pmatrix} l & \lambda & l_0\\ 0 & 0 & 0\end{pmatrix}$$

$$\times(-)^{L_0+L+L_c+S_0+J_0+J}(\hat{J}_0\hat{J}\hat{L}_0\hat{L})^{1/2}\begin{Bmatrix}\lambda & J & J_0\\ S_0 & L_0 & L\end{Bmatrix}\begin{Bmatrix}\lambda & L & L_0\\ L_c & l_0 & l\end{Bmatrix}g^{B}_{\lambda}(K)\ , \quad (22)$$

where

$$g^{B}_{\lambda}(K)=\langle R_{nl}(r)\,|j_{\lambda}(Kr)|R_{n_0l_0}(r)\rangle\ . \quad (23)$$

In Eq. (22), the arrays in curly brackets are $6j$ symbols.[19] In applying Eq. (22) to the pure Born term T_6 of Eq. (14), we choose the direction of $\hat{K}$ as the z axis.

D. Evaluation of $T_1,\ldots,T_6$

The quantities $T_1,\ldots,T_6$, which determine the differential cross sections, may now be calculated using Eq. (16) with ξ^{λ} replaced by $\xi^{\lambda}-\xi^{B\lambda}$ for M^D-M^B, and the expressions (19) and (22) for M^E and M^B. We omit the tedious but straightforward details and proceed to the final results:

$$T_1=\sum_p(-)^p\sum_{\lambda}\frac{\hat{L}}{\hat{\lambda}}\begin{Bmatrix}\lambda & L & L_0\\ L_c & l_0 & l\end{Bmatrix}^2\sum_{\substack{l_il_f\\ \bar{l}_i\bar{l}_f}}c_{p\lambda}(l_il_f,\bar{l}_i\bar{l}_f)\times g^{\lambda l_il_f}_{S_cL_c}g^{\lambda\bar{l}_i\bar{l}_f*}_{S_cL_c}P_p(\cos\theta)\ , \quad (24)$$

$$T_2=\sum_p(-)^p\sum_{\lambda}\hat{L}(-)^{\lambda+1}\begin{Bmatrix}\lambda & L & L_0\\ L_c & l_0 & l\end{Bmatrix}^2\times\sum_{\substack{l_il_f\\ \bar{l}_i\bar{l}_f}}c_{p\lambda}(l_il_f,\bar{l}_i\bar{l}_f)\,\mathrm{Re}(g^{\lambda l_il_f}_{S_cL_c}h^{\lambda\bar{l}_i\bar{l}_f*}_{S_cL_c})\,P_p(\cos\theta)\ , \quad (25)$$

$$T_3=\sum_p(-)^p\sum_{\lambda}\hat{L}\hat{\lambda}\frac{\hat{S}}{2\hat{S}_c}\begin{Bmatrix}\lambda & L & L_0\\ L_c & l_0 & l\end{Bmatrix}^2\times\sum_{\substack{l_il_f\\ \bar{l}_i\bar{l}_f}}c_{p\lambda}(l_il_f,\hat{l}_i\hat{l}_f)h^{\lambda l_il_f}_{S_cL_c}h^{\lambda\bar{l}_i\bar{l}_f*}_{S_cL_c}P_p(\cos\theta)\ , \quad (26)$$

$$T_4=4\pi\sum_{\lambda l_il_f}i^{l_i-l_f-\lambda}(-)^{l_f}\frac{2}{\hat{\lambda}}\begin{Bmatrix}\lambda & L & L_0\\ L_c & l_0 & l\end{Bmatrix}^2\times\mathcal{Y}^{l_il_f}_{\lambda}(\theta)\,\mathrm{Re}(g^{\lambda l_il_f}_{S_cL_c})\,\mathcal{G}^{\lambda B}(K)\ , \quad (27)$$

$$T_5=4\pi\sum_{\lambda l_il_f}i^{l_i-l_f-\lambda}(-)^{l_f+\lambda+1}\begin{Bmatrix}\lambda & L & L_0\\ L_c & l_0 & l\end{Bmatrix}^2\times\mathcal{Y}^{l_il_f}_{\lambda}(\theta)\,\mathrm{Re}(h^{\lambda l_il_f}_{S_cL_c})\,\mathcal{G}^{\lambda B}(K)\ , \quad (28)$$

$$T_6=\sum_{\lambda}\frac{1}{\hat{L}}\begin{Bmatrix}\lambda & L & L_0\\ L_c & l_0 & l\end{Bmatrix}^2[\mathcal{G}^{\lambda B}(K)]^2\ , \quad (29)$$

where

$$c_{p\lambda}(l_il_f,\hat{l}_i\hat{l}_f)=i^{l_i-l_f-\bar{l}_i+\bar{l}_f}(-)^{\lambda}(\hat{l}_i\hat{l}_f\hat{\bar{l}}_i\hat{\bar{l}}_f)^{1/2}\times(l_f0\bar{l}_f0|p0)\,(l_i0\bar{l}_i0|p0)\times\begin{Bmatrix}l_i & \lambda & l_f\\ \bar{l}_f & p & \bar{l}_i\end{Bmatrix}\ , \quad (30)$$

$$g^{\lambda l_i l_f}_{S_c L_c} = \mathfrak{F}(-)^{l_i+l_0}\,(\hat{l}_f)^{1/2}\,(l_f 0\lambda 0\,|\,l_i 0) \times(\xi^{\lambda}_{l_i l_f l l_0} - \xi^{B\lambda}_{l_i l_f l l_0})\,, \quad (31)$$

$$\mathfrak{F} = (4\pi N\hat{l}_0)^{1/2}\,F^{S_0 L_0}_{S_c L_c}\,(l_0 0\lambda 0\,|\,l 0)\,, \quad (32)$$

$$h^{\lambda l_i l_f}_{S_c L_c} = (4\pi N\hat{l}\hat{l}_0)^{1/2}\,F^{S_0 L_0}_{S_c L_c}\sum_{\beta}(-)^{\beta}\,(l_0 0\beta 0\,|\,l_f 0) \times(l 0\beta 0\,|\,l_i 0)\begin{Bmatrix} l_0 & l & \lambda \\ l_i & l_f & \beta \end{Bmatrix}\eta^{\beta}_{l_i l_f l l_0}\,, \quad (33)$$

$$\mathcal{G}^{\lambda B}(K) = \mathfrak{F}(-)^{l}\,(\lambda)^{1/2}\,\hat{L}K^{-2}g^{B}_{\lambda}(k)\,, \quad (34)$$

$$\mathcal{Y}^{l_i l_f}_{\lambda}(\theta) = \sum_{m}(l_f - m\lambda m\,|\,l_i 0)\,Y_{l_f -m}(\hat{k}_f)\,Y_{\lambda m}(\hat{K})\,. \quad (35)$$

In Eqs. (24)–(26), $P_p(\cos\theta)$ is a Legendre polynomial. The quantities $\xi^{\lambda}_{l_i l_f l l_0}$, $\xi^{B\lambda}_{l_i l_f l l_0}$, $\eta^{\beta}_{l_i l_f l l_0}$, and $g^{B}_{\lambda}(K)$ which appear in Eqs. (31), (33), and (34) are the radial matrix elements (17), (18), (20), and (23).

E. Integrated Cross Section

The integrated cross section $\sigma = \int (d\sigma/d\Omega)\,d\Omega$ is expressible in the form

$$\sigma = \delta_{SS_0}(\sigma_1 + \sigma_2 + \sigma_4 + \sigma_5 + \sigma_6) + \sigma_3\,, \quad (36)$$

where

$$\sigma_j = 2\pi\gamma\int_{-1}^{1} T_j\,d(\cos\theta), \qquad j = 1, \ldots, 6\,. \quad (37)$$

We find

$$\sigma_j = a_0^2(4k_f/k_i)B_{j,0} \qquad \text{for } j = 1, 2, 3, \quad (38)$$

where $B_{j,0}$ is the coefficient of $P_0(\cos\theta)$ in T_j in (24)–(26) for $j = 1, 2, 3$ and

$$\sigma_j = a_0^2(2/k_i^2)\int_{K_l}^{K_u} T_j K\,dK \qquad \text{for } j = 4, 5, 6\,, \quad (39)$$

where $K = (k_i^2 + k_f^2 - 2k_i k_f\cos\theta)^{1/2}$ and $K_{u,l} = k_i \pm k_f$.

F. Additional Remarks

The final expression for the differential cross section, Eq. (7), when Eqs. (24)–(29) are substituted in, does not depend on J_0. Thus, for the ground-state members $^3P_0$, $^3P_1$, and $^3P_2$ of atomic oxygen, for example, we obtain the same results. In fact, by averaging over contributions from all three states, we find the same expression for the differential cross sections as given here, if we ignore the small energy splittings as we do here.

The multipole order λ for the $p \to s$ and $p \to p$ transitions that can contribute are listed in Table I, together with the possible final-orbital angular momenta l_f that are coupled to a given initial-orbital angular momentum l_i of the projectile. The table also contains the multipole order β that can contribute in the sum appearing in the exchange amplitude $h^{\lambda l_i l_f}_{S_c L_c}$ of Eq. (33). The last column in Table I indicates the terms T_1–T_5 that contribute for each classification.

TABLE I. Multipole orders and l_f for the $p \to s$ and $p \to p$ transitions.

Transition	λ	l_f[a]	β	Contributing terms
$p \to s$	1	$l_i \pm 1$	l_i	T_1, T_2, T_3, T_4, T_5
$p \to p$	2	$l_i - 2$	$l_i - 1$	
		l_i	$l_i \pm 1$	
		$l_i + 2$	$l_i + 1$	T_1, T_2, T_4, T_5
	0	l_i	$l_i \pm 1$	
	1	l_i	$l_i \pm 1$	T_3

[a]For $\lambda = 2$, if $l_i = 0$, we have $l_f = 2$ only, and if $l_i = 1$, we have $l_f = 1$ and 3 only. Similarly, for $\lambda = 1$ in $p \to p$, no $l_i = l_f = 0$ is allowed.

The coefficients $c_{p\lambda}(l_i l_f, \hat{l}_i \hat{l}_f)$ defined by Eq. (30) satisfy the symmetry property given by Eq. (3.27) of SPG. This property is utilized to greatly economize the fourfold sums over $l_i l_f \hat{l}_i \hat{l}_f$ that appear in T_1, T_2, and T_3.

The asymptotic forms of the distorted radial wave functions $f_{l_i}(k_i, r)$ and $f_{l_f}(k_f, r)$ are given by Eq. (3.6) of SPG. In computing the radial matrix element $g^{\lambda l_i l_f}_{S_c L_c}$ of Eq. (31) for direct amplitude, we must cut off the integral at some practical point $r_{\max}$, where f_{l_i} and f_{l_f} have attained their asymptotic forms. Owing to the extreme long-range nature of the form factor $\langle R_{nl}(r_1)\,|\,r_<^{\lambda}/r_>^{\lambda+1}\,|\,R_{n_0 l_0}(r_1)\rangle$ that appears in Eqs. (17) and (18), the error committed by ignoring the contribution from $r > r_{\max}$ is not negligible unless $r_{\max}$ is chosen extremely large. This problem is peculiar to the direct amplitude and does not arise for the exchange amplitude. In order to achieve a sufficient numerical accuracy and yet maintain the computational economy, we proceed as explained in SPG: For lower partial waves, we replace f_{l_i} and f_{l_f} for $r > r_{\max}$ by their sinusoidal asymptotic forms and convert the integrals involving the form factor in their integrands into sums of quickly converging series of integrals, each integral ranging over a period of sine or cosine functions. This method is particularly suited for the computation of $M^D - M^B$, since for higher partial waves, for which f_{l_i} and f_{l_f} have not attained their sinusoidal asymptotic forms at $r_{\max}$, the errors tend to cancel between ξ^{λ} and $\xi^{B\lambda}$.

III. CHOICE OF IPM POTENTIALS

We apply the formulation presented in Sec. II to the electron-impact excitation of atomic oxygen in which an electron in the $2p$ shell is excited to $3s$, $3p$, and $4p$ shells. These bound electrons are assumed to be in the IPM potential of the form[10]

$$V_B(r) = -\frac{2}{r}\left(\frac{Z-1}{H(e^{r/d}-1)+1}+1\right), \qquad (40)$$

where $Z = 8$ and the values of the parameters are those of KGG:

$$d = 0.8164, \quad H = 2.224 \quad \text{(KGG)}.$$

In this work, we employ rydberg units unless otherwise specified (1 Ry = 13.6 eV). As explained in the Introduction, this potential reproduces the single-particle levels of atomic oxygen quite well.[15] In particular, the binding energies of $2p$, $3s$, $3p$, and $4p$ electrons in this potential are 1.0031, 0.3050, 0.1950, and 0.0929 Ry, respectively. As in SPG, we utilize $V_B(r)$ also as the distorting potential for the exchange amplitude to avoid unphysically large exchange contributions arising from the nonorthogonality of scattering and bound states, and to maintain the post-prior symmetry of the exchange amplitude.

For the direct amplitude, we employ a distorting potential with a form similar to $V_B(r)$ but without the Coulomb tail[10]:

$$V(r) = -\frac{2}{r}\,\frac{Z}{H(e^{r/d}-1)+1}. \qquad (41)$$

The parameter set KGG, when used in (41), is found to produce a large p-wave-shape resonance. The total cross section σ_T predicted by this potential has a peak at ~ 4 eV with the value ~ $140a_0^2$ (a_0 is the Bohr radius) and a half-width ~ 3 eV. The experimental σ_T measured by Sunshine *et al.*[17] as plotted in Fig. 1 does not possess such a huge resonance. Apparently, the elastic channel seems to demand a somewhat different set of parameters than KGG. The inclusion of a phenomenological polarization potential is a possible way of eliminating this resonance. However, then the DW calculation becomes prohibitive owing to the extreme long-range nature of the polarization potential. In order to be compatible with the measured σ_T and yet to keep the computation practical, and hopefully to simulate the effect of the polarization potential to some extent, we modify the potential by gradually increasing d from 0.8164, fixing H to 2.224, until we obtain a reasonable agreement with the experimental σ_T. The variation of σ_T as a function of d is shown in Fig. 1. An increase in d by ~ 25% eliminates the resonance completely, bringing down the predicted σ_T to the experimental level. We choose as the modified parameters of the distorting potential

$$d = 0.9900, \quad H = 2.224 \quad \text{(set SG1)}$$

to be used for the direct amplitude. The predicted σ_T by this potential lies somewhat lower than the data at energies above ~ 10 eV, as can be seen from Fig. 1. This may be desirable rather than objectionable, since we use a purely real potential, and hence no processes other than elastic scattering are accounted for. At present, in view of the complete lack of data on elastic differential cross sections, we feel that the use of a complex optical-model potential is not warranted.

In any event, a certain degree of arbitrariness is unavoidable at this time for the phenomenological determination of the distorting potential. To study the sensitivity of the results of the DW calculation on the choice of parameters in Sec. IV, we present an alternative set to be used in $V(r)$ for the direct amplitude:

$$d = 1.250, \quad H = 3.150 \quad \text{(set SG2)}.$$

The predicted σ_T by this potential is also shown in Fig. 1.

As in SPG, we use the same distorting potential $V(r)$ for the outgoing channel as for the incident channel, although, strictly speaking, the incoming and outgoing electrons should be in somewhat different atomic fields. The results presented in Sec. IV utilize the potential $V_B(r)$ of Eq. (40) with the parameter set KGG for the computations of the bound-state wave functions and the scattering states in the exchange amplitude. The scattering states in the direct amplitude are computed by using $V(r)$ of Eq. (41) with the parameter sets KGG, SG1, and SG2.

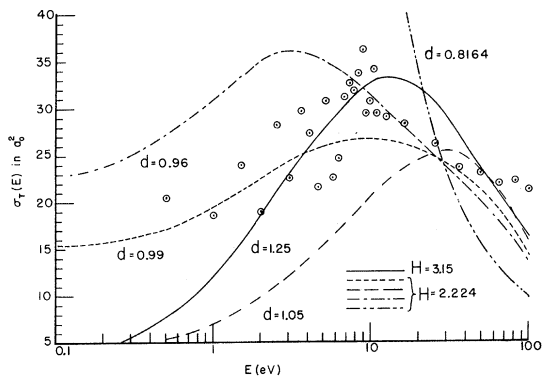

FIG. 1. Total cross section $\sigma_T(E)$. Circles are the experimental data of Sunshine *et al.* (Ref. 17). Curves are the theoretical values obtained by using the potential $V(r)$ of Eq. (41) with the parameters as indicated in the figure.

IV. RESULTS AND DISCUSSION

In presenting the angular distributions we define the distorted generalized oscillator strength (DGOS) by

$$f_d(x,E) = \frac{k_i}{4k_f}\,\frac{x}{a_0^2}\,x_t \sum_J \frac{d\sigma}{d\Omega}, \qquad (42)$$

where E is the incident energy and $x = K^2a_0^2$. The

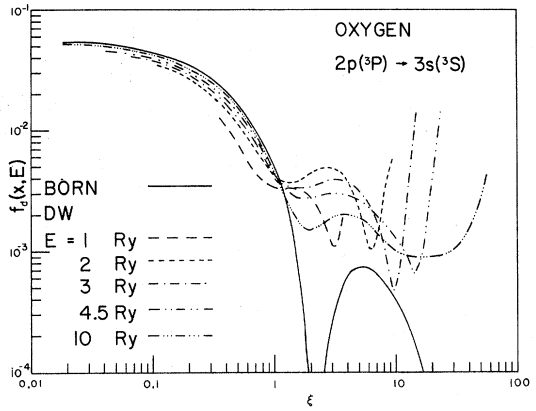

FIG. 2. DGOS for $2p(^3P) \rightarrow 3s(^3S)$ with the SG1 parameters. Except for the Born prediction shown by the solid curve, the beginning and the end of each curve correspond to the 0° and 180° scattering, respectively.

quantity x_t is the excitation energy in rydbergs. At high energies, the DGOS approaches the generalized oscillator strength (GOS), which is a function of x only. In plotting DGOS, we use the scaled variable $\xi = x/x_t$ instead of x.

The theoretical predictions of DGOS as a function of ξ for various values of E obtained with SG1 are shown in Figs. 2 and 3 for the $2p \rightarrow 3s(^3S)$ and $3p(^3P)$ transitions. (As explained in Sec. III, the bound states and exchange amplitude are computed with KGG.) The Born limits (GOS) are also shown in Figs. 2 and 3. The results of the $3s(^3S)$ excitation shown in Fig. 2 are reminiscent of the results obtained for Ne previously.[13] Extrapolating GOS to zero-momentum transfer, we find the optical oscillator strength for this transition to be 0.056. Comparison with the experimental optical oscillator strengths[20–27] given in Table II shows that, although the experimental values vary considerably, our value is centrally located with respect to these

TABLE II. Experimental optical oscillator strengths for the $2p$–$3s$ transition in atomic oxygen.

Ref.	Optical oscillator strength
20	0.033
21	0.033
22	0.035
23	0.023
24	0.18
25	0.050
26	0.046
27	0.044
Present work	0.056

determinations. The results shown in Fig. 3 for $3p(^3P)$ exhibit the characteristic feature of an optically forbidden transition, approaching zero as ξ goes to zero.

The results for DGOS of the $4p(^3P)$ excitation are quite similar to Fig. 3 in their ξ and E dependence, except that the magnitudes are about $\frac{1}{4}$ of the $2p \rightarrow 3p$ transition.

The predicted DGOS for the $2p \rightarrow 3s(^5S)$ and $3p(^5P)$ transitions are presented in Figs. 4 and 5. These transitions are of purely exchange origin in our model, and, as such, the values of DGOS vanish rapidly with increasing energy. For these transitions, KGG, SG1, and SG2 give identical results, because the KGG parameters are always used for the calculation of exchange amplitudes.

The sensitivity of the predicted DGOS to the choice of the distorting potential may be studied by comparing the results from different potentials which yield comparable fits to the experimental total cross section shown in Fig. 1. The results with the alternative set SG2 are shown in Figs. 6 and 7. Despite the large difference between SG1 and SG2, these models give rather similar results for the DGOS as a function of E and ξ. This suggests that our results may be insensitive to the

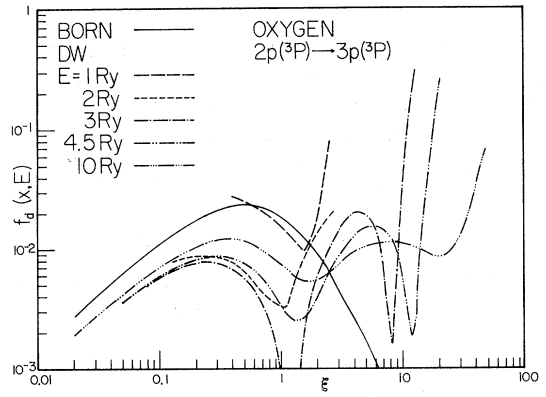

FIG. 3. DGOS for $2p(^3P) \rightarrow 3p(^3P)$ with SG1. See the caption of Fig. 2.

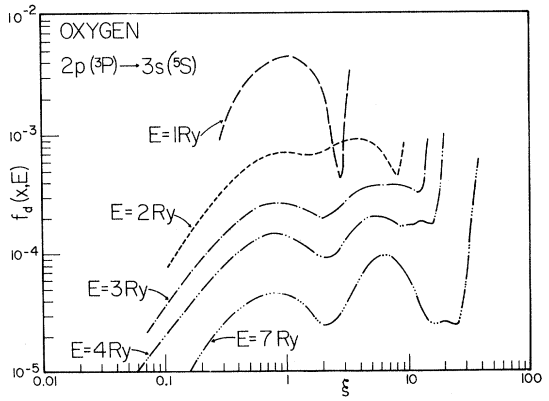

FIG. 4. DGOS for $2p(^3P) \rightarrow 3s(^5S)$.

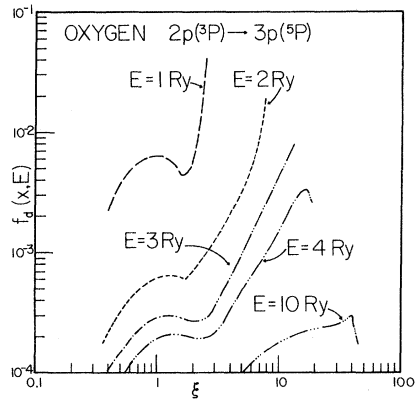

FIG. 5. DGOS for $2p(^3P) \rightarrow 3p(^5P)$.

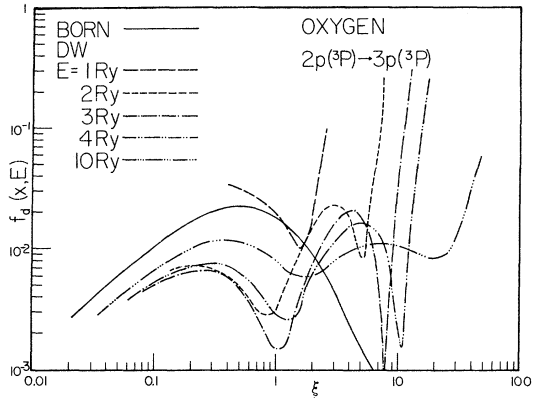

FIG. 7. DGOS for $2p(^3P) \rightarrow 3p(^3P)$ with SG2. See the caption of Fig. 2.

choice of the distorting potential provided that it is consistent with the experimental total cross sections.

As seen from Figs. 2, 3, 6, and 7, the effects of distortion remain large even at energies as high as 10 Ry, especially at large angles. The effects of exchange are readily seen from Figs. 4 and 5 for quintet states which are of purely exchange origin. As noted earlier, the exchange effects diminish rapidly with increasing energy.

In Fig. 8, we show the integrated cross section $\sigma(E)$ summed over all the triplet transitions considered. The contributions to $\sigma(E)$ from individual transitions are given in Table III. Recently, Stone and Zipf[18] have measured the resonance radiation at 1304 Å emitted after the electron-impact excitation of atomic oxygen from the threshold to 150 eV, and extracted the total cross section for the $3s(^3S)$-$2p(^3P)$ emission. Their results are also shown in Fig. 8 by a solid curve. The sharp peak observed near 15 eV is attributed by Stone and Zipf to the population of the ^3S state by cascade radiation from the $4p(^3P)$ and $3p(^3P)$ states. They estimate the absolute magnitude of the total cross section for direct excitation of the $3p(^3P)$ and $4p(^3P)$ states to be about 1.2×10^{-16} cm^2 at its peak near 17 eV, and that for the $3s(^3S)$ to be about 2.1×10^{-17} cm^2 at its peak near 50 eV. If we assume that all direct excitations of the $4p$ level lead to population of the $3s$ level, we may compare our result summed over $3s(^3S)$, $3p(^3P)$, and $4p(^3P)$ with the results of Stone and Zipf.[18] This assumption is not strictly correct, since the $4p$ level can decay via $3d$ and $4s$ levels which can both go directly to the ground state. As seen from Fig. 8, our result is in reasonable agreement with their data for $E \gtrsim 2$ Ry, but the low-energy peak is not reproduced at all. The predicted $\sigma(E)$ for the ^3P transition is not as sharply peaked at low energy as suggested by Stone and Zipf. In Fig. 8 and Table III we also present the

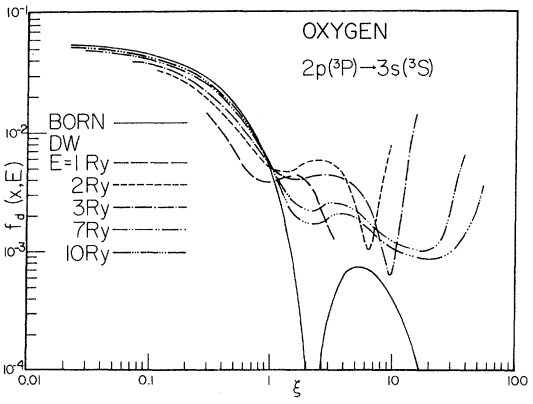

FIG. 6. DGOS for $2p(^3P) \rightarrow 3s(^3S)$ with SG2. See the caption of Fig. 2.

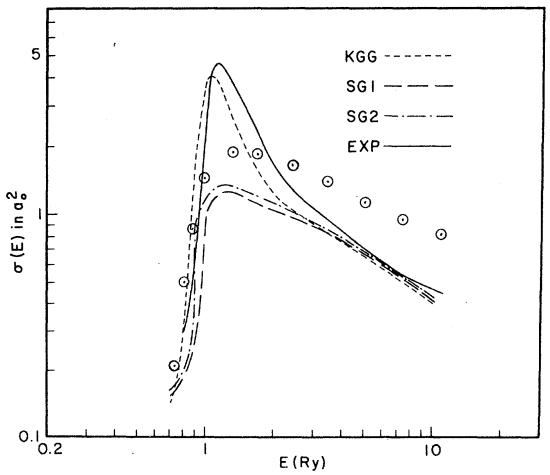

FIG. 8. Integrated cross section $\sigma(E)$ summed over the $3s(^3S)$, $3p(^3P)$, and $4p(^3P)$ final states. The experimental data of Stone and Zipf (Ref. 18) are represented by the solid curve. The symbol ⊙ refers to the experimental data of Zipf (Ref. 28).

TABLE III. Integrated cross sections $\sigma(E)$ in a_0^2.

	E (Ry)	1	1.5	2	3	4.5	7	10
SG1	$3s(^3S)$	0.225	0.391	0.442	0.435	0.385	0.315	0.261
	$3p(^3P)$	0.619	0.569	0.488	0.367	0.256	0.165	0.115
	$4p(^3P)$	0.132	0.145	0.124	0.094	0.066	0.042	0.030
	$3s(^5S)$	0.126	0.049	0.023	0.007	0.002	0.001	0.000
	$3p(^5P)$	0.201	0.085	0.047	0.020	0.008	0.002	0.001
	$4p(^5P)$	0.072	0.029	0.016	0.007	0.002	0.001	0.000
	E (Ry)	1	2	3	4	4.5	7	10
SG2	$3s(^3S)$	0.230	0.449	0.438	0.403	...	0.316	0.261
	$3p(^3P)$	0.767	0.521	0.375	0.288	...	0.165	0.115
	$4p(^3P)$	0.168	0.133	0.096	...	0.066	0.042	0.030
	E (Ry)	1	1.5	2	3	4.5	7	10
KGG	$3s(^3S)$	0.583	0.360	0.419	0.432	0.386	0.316	0.261
	$3p(^3P)$	2.751	1.180	0.624	0.371	0.247	0.160	0.112
	$4p(^3P)$	0.250	0.363	0.170	0.096	0.063	0.041	0.029

predicted $\sigma(E)$ using the KGG parameters. Owing to the p-wave-shape resonance present in this potential, the theoretical $\sigma(E)$ shows a large peak near threshold quite compatible with the data. Unfortunately, we have to reject this solution in view of the difference between the predicted and experimental total cross section σ_T as discussed in Sec. III. These considerations suggest that at energies below ~2 Ry our model is not accurate enough to reproduce simultaneously the total cross section σ_T of Sunshine *et al.*[17] and the integrated cross section $\sigma(E)$ of Stone and Zipf.[18] Also shown in Fig. 8 are the most recent data of Zipf.[28] The E dependences of our DW predictions with SG1 and SG2 are quite similar to these recent data, although the magnitudes are smaller by a factor of 2. The discrepancy between our DW results and the experimental data would worsen if the $3p(^3P)$ state does not have a pure parent state ^4S but has a mixture of ^4S and ^2D as suggested by Percival.[8]

To summarize, the DW calculation presented here for atomic oxygen shows that the effects of distortion on angular distributions are quite important even at energies as high as 10 Ry, and that, nevertheless, for the integrated cross sections, the Born approximation seems to hold quite well even at lower energies. This latter result is due to the compensation between the contributions to the cross sections from the backward and forward angles, these contributions being, respectively, larger and smaller than those given by the Born approximation. At energies below ~2 Ry, our theory is incapable of reproducing the integrated cross section of Stone and Zipf.[18] At low energies we may have to consider the polarization effect explicitly. It is highly desirable that calculations with the close-coupling approach using the formulation, for example, of Smith and Morgan[29,30] be performed in order that one may compare the merits of the DW approximation with those of the close-coupling theory for the transitions considered here. For the entire energy range considered, the E dependence of our theoretical prediction on the integrated cross section $\sigma(E)$ is in reasonable agreement with the recent data of Zipf.[28] It is hoped that our results on DGOS and $\sigma(E)$ are useful in applications such as microscopic studies of electron-energy deposition.

ACKNOWLEDGMENTS

The authors would like to thank Professor A. E. S. Green for suggesting the problem to us and for his continued support and interest during the course of this work. One of us (P.S.G.) would like to express his appreciation to Professor Green for making possible his visit to the University of Florida. The authors are grateful to Professor E. C. Zipf for making his experimental data available prior to publication.

*Work supported in part by the Air Force Office of Scientific Research and the National Science Foundation.

†On leave from the California State University, Los Angeles, Calif. 90032.

[1]B. L. Moiseiwitsch and S. J. Smith, Rev. Mod. Phys. 40, 238 (1968).

[2]H. S. W. Massey and E. H. S. Burhop, *Electronic and Ionic Impact Phenomena* (Clarendon, Oxford, England, 1969), Vol. 1.

[3]T. Yamanouchi, T. Inui, and A. Amemiya, Proc. Phys.-Math. Soc. Japan 22, 847 (1940); T. Yamanouchi and M. Kotani, Proc. Phys.-Math. Soc. Japan 22, 14

(1940).
[4]M. J. Seaton, Phil. Trans. Roy. Soc. London A245, 469 (1953); M. J. Seaton, Proc. Roy. Soc. (London) A231, 37 (1955).
[5]K. Smith, R. J. W. Henry, and P. G. Burke, Phys. Rev. 157, 51 (1967).
[6]R. J. W. Henry, P. G. Burke, and A. L. Sinfailam, Phys. Rev. 178, 218 (1969).
[7]D. R. Bates, A. Fundaminsky, J. W. Leech, and H. S. W. Massey, Phil. Trans. Roy. Soc. London A243, 93 (1950).
[8]I. C. Percival, Proc. Phys. Soc. (London) A70, 241 (1957).
[9]A. D. Stauffer and M. R. C. McDowell, Proc. Phys. Soc. (London) A89, 289 (1966).
[10]A. E. S. Green, D. L. Sellin, and A. S. Zachor, Phys. Rev. 184, 1 (1969).
[11]J. E. Purcell, R. A. Berg, and A. E. S. Green, Phys. Rev. A 2, 107 (1970); 3, 509 (1971).
[12]P. S. Ganas and A. E. S. Green, Phys. Rev. A 4, 182 (1971).
[13]T. Sawada, J. E. Purcell, and A. E. S. Green, Phys. Rev. A 2, 193 (1971).
[14]R. A. Berg and A. E. S. Green, Adv. Quantum Chem. (to be published).
[15]P. A. Kazaks, P. S. Ganas, and A. E. S. Green, Phys. Rev. A 6, 2169 (1972).
[16]W. N. Shelton and E. S. Leherissey (report of work prior to publication, 1971).
[17]G. Sunshine, B. B. Aubrey, and B. Bederson, Phys. Rev. 154, 1 (1967).
[18]E. J. Stone and E. C. Zipf, Phys. Rev. A 4, 610 (1971).
[19]A. Messiah, *Quantum Mechanics* (Wiley, New York, 1965). The conventions for the angular-momentum couplings used throughout this work are those of this book.
[20]A. B. Prag, C. E. Fairchild, and L. C. Clarn, Phys. Rev. 137, A1358 (1965).
[21]F. A. Morse and F. Kaufman, J. Chem. Phys. 42, 1785 (1965).
[22]B. D. Savage and G. M. Lawrence, Astrophys. J. 146, 940 (1966).
[23]D. A. Parkes, L. F. Keyser, and F. Kaufman, Astrophys. J. 149, 217 (1967).
[24]G. Boldt and F. Labuhn, Z. Naturforsch. A22, 1613 (1967).
[25]J. E. Hesser, J. Chem. Phys. 48, 2518 (1968).
[26]G. M. Lawrence and M. George, Phys. Rev. 175, 40 (1968).
[27]C. Lin, D. A. Parkes, and F. Kaufman, J. Chem. Phys. 53, 3896 (1970).
[28]E. C. Zipf (private communication).
[29]K. Smith and L. A. Morgan, Phys. Rev. 165, 110 (1968).
[30]S. P. Rountree and R. J. W. Henry, Phys. Rev. Abstracts 3, 5 (1972).

PHYSICAL REVIEW A VOLUME 7, NUMBER 2 FEBRUARY 1973

Impact-Parameter Theory Defined as a Constant-Collision-Velocity Semiclassical Limit of a Complete Quantum-Scattering Picture

Merle E. Riley
Sandia Laboratories, Albuquerque, New Mexico 87115
(Received 21 September 1972)

A semiclassical limit, defined in terms of large mass and energy at fixed arbitrary collision velocity, is shown to be a simple formal prescription for obtaining a quantum treatment of the impact-parameter method and the eikonal approximation. In particular, for atom-atom collisions, the resultant approximation is emphasized to be a proper strong-coupling equation for inelastic processes, as opposed to the adiabatic result of a large-mass limit at fixed energy.

I. INTRODUCTION

Semiclassical analysis and perturbation theory are two systematic means of obtaining approximate solutions in quantum mechanics to complex problems. This paper presents an argument for the recognition of a semiclassical limit distinct from the usual large-mass limit[1]; the new limit is called isovelocity for it is taken at large mass with fixed velocity rather than fixed energy. The usual semiclassical limit involves the construction of an asymptotic solution[2] of an ordinary differential equation,

$$\left(\alpha^2 \frac{d^2}{dr^2} + K^2(r)\right)\psi(r, \alpha) = 0 , \qquad K^2(r) = (2\mu/\hbar^2)[E - V(r)] , \tag{1}$$

as the dimensionless parameter α becomes small. α is sometimes associated with the physical constant $\hbar$, but an association with the mass μ, defined by replacing μ by μ/α^2 in the Schrödinger equation, is advantageous because it immediately shows that the asymptotic solutions are better for a proton than for a positron with the same energy in a given potential field. This paper will concern